The Non-Linear Response of a Two-Layer, Baroclinic Ocean to a Stationary, Axially-Symmetric Hurricane: Part I. Upwelling Induced by Momentum Transfer[1]

JAMES J. O'BRIEN

National Center for Atmospheric Research, Boulder, Colo.

AND ROBERT O. REID

Texas A&M University, College Station

(Received 21 June 1966)

ABSTRACT

This study is concerned with the theoretical description of upwelling induced in a stratified, rotating, two-layer ocean by momentum transfer from an intense stationary, axially-symmetric atmospheric vortex. The dynamic internal response of the ocean is assumed to be axially-symmetric which permits consideration of the solution in two independent variables, radial distance and time. Numerical integration via the method of characteristics is utilized to obtain values of radial velocity, tangential velocity, and depth of the upper layer for a period of two days. Transfer of momentum between the air and the sea and between the upper and lower layers are allowed. Transfer of heat and moisture with the atmosphere is not considered.

A general model is derived which leads to a hierarchy of models of increasing complexity. The detailed solution of the first of these is illustrated.

Results agree qualitatively with observations taken in the Gulf of Mexico following hurricane Hilda, 1964. Intense upwelling is confined to within twice the radius of maximum winds. The displaced warm central waters produce some downwelling adjacent to the upwelled region. The degree of upwelling is time-dependent and the hurricane-force winds must act on the ocean for several hours before significant upwelling occurs. The model indicates a strong coupling of the radially propagating internal wave mode and the vortex mode of the system. This coupling confines the significant internal disturbances to within the wind-forced region.

1. Introduction

The present investigation is concerned with a particular aspect of the general problem of air-sea interaction, specifically, the theoretical description of upwelling induced in a stratified, rotating ocean by an intense hurricane. Attention is confined to the time-dependent response of a two-layer ocean over which there is a stationary, axially-symmetric atmospheric vortex. The dynamic response of the ocean to the cyclone is assumed to be axially symmetric, which permits consideration of the solution in cylindrical coordinates as a function of only two independent variables, radial distance and time. This implies that scales of motion comparable to surface waves and smaller scales are ignored explicitly in the model. Effects of small scale turbulent processes are included implicitly by consideration of mixing and the vertical transfer of momentum.

The dependent variables are depth, density, and the depth-averaged radial and tangential velocities in both upper and lower layers of the ocean. The radial distributions of atmospheric surface pressure and atmospheric turbulent shear stresses are prescribed. Transfer of momentum between the air and sea and between the upper and lower layers is included. However, transfer of sensible heat or latent heat between the model ocean and the atmosphere is not considered. An initial state of rest is stipulated for the laterally-infinite, homogeneous ocean layers.

Within this framework, it is possible to consider a hierarchy of models of increasing complexity which can be studied separately. The present paper includes the development of the general model and describes the detailed solution of one specific model. This model permits momentum transfer between the air and the sea as well as between the two ocean layers. A subsequent paper will describe a similar model which considers the additional effect of turbulent mixing of heat and salt between the ocean layers. This second paper will also compare various energy integrals of the two models.

This investigation was inspired by observations taken by Leipper (1967) who reported an observed decrease of over 5C of sea surface temperature in an area of 15,000 mi^2 following the passage of hurricane Hilda, 1964, in the central Gulf of Mexico. He displayed vertical sections perpendicular to the hurricane's path which when compared to undisturbed sections, showed the changes in temperature and salinity which appeared

[1] A part of this paper was presented at the 47th Annual Meeting of the American Geophysical Union, Washington, D. C., April 1966.

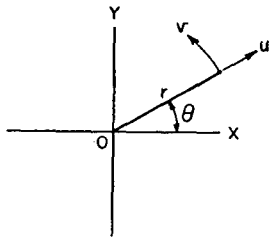

SCHEMATIC OF COORDINATES AND VELOCITY COMPONENTS

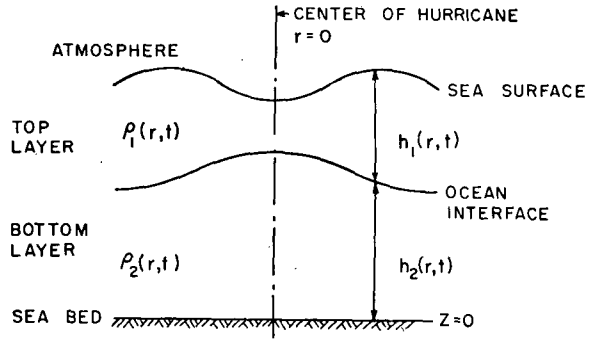

FIG. 1. Geometry of the hurricane-ocean system. The lower diagram represents any radial cross section. In addition, $h_2 \gg h_1$.

to be the result of the storm's action on the ocean. The warm surface waters were displaced to either side of the cyclone path and a core of cold water appeared near the center of the wake, suggesting active upwelling in the latter region. Vertical displacement of isotherms of the order of 60 m occurred near the center. His observations will be compared with the results of the present work.

Leipper's measurements are the most striking evidence of the phenomenon; however, there are additional observations. Fisher (1958) and Jordan (1964), using routine ship observations averaged over 1 day and 15 days, respectively, indicate that low sea surface temperatures are often found in the wake of intense atmospheric cyclones. Hidaka and Akiba (1955) and Ichiye (1955) refer to occurrences of cold surface waters near Japan following the passage of typhoons.

There are several processes which may contribute to the lowering of sea surface temperatures. Jordan (1964) estimated that, in the presence of a deep mixed layer, the maximum sea surface temperature decrease which can be accounted for by processes such as precipitation, evaporation, and sensible and turbulent heat transfer in 72 hr is 2F.

It is expected, *a priori*, that the ocean's initial dynamic and thermodynamic response to a hurricane would be to produce a well-mixed, isothermal surface layer which usually would lead to some cooling of the sea surface. However, it appears that only upwelling of cold deep water can explain the extreme cooling found by Leipper after Hilda. The previous theoretical studies are reviewed and compared with the present work in a later section.

2. Formulation of a general model

Consider a two-layer ocean in a laterally-infinite region of uniform undisturbed depth. The fluid densities within the upper and lower layers are designated respectively by ρ_1 and ρ_2, where $\rho_2 > \rho_1$. (See list of symbols at end of paper.) A schematic drawing of the geometry of the model is shown in Fig. 1. A cylindrical coordinate system is chosen such that the radial coordinate r is zero at the center of the axially-symmetric atmospheric cyclone and increases outward. The vertical coordinate z is zero at the horizontal sea bed and increases upward. The instantaneous thicknesses of the upper and lower layers are denoted, respectively, by h_1 and h_2. These thicknesses and the densities, ρ_1 and ρ_2, are taken to be functions of r and t but not of z.

The fundamental assumptions imposed on the complete hydrodynamic differential equations are:

a) The dynamic response to the axially-symmetric atmospheric cyclone is assumed to be axially symmetric, i.e., independent of the azimuth coordinate θ.

b) The horizontal velocities are assumed to be independent of depth in each layer. (Thus, they can be regarded as corresponding to the vertically-averaged values of velocity of an actual system.)

c) The vertical distribution of pressure is hydrostatic. (This implies that we confine attention to disturbances of fairly large wavelength.)

d) The traditional Coriolis approximations are assumed and the Coriolis parameter f is constant.

e) Both molecular and turbulent lateral friction are neglected.

f) There is no exchange of mass or heat between the atmosphere and the ocean. That is, evaporation, precipitation, sensible and turbulent heat transfer, and radiation exchange with the air are neglected.

It should be recognized that the variation of the Coriolis parameter f with latitude may produce asymmetrical motions aside from the modeling assumption that the response to the external torque applied by the wind stress is axially symmetric. However, the results of the numerical models will be compared with actual east-west cross sections following hurricane Hilda and, therefore, the approximation, f is constant, is retained.

The problem is to derive the changes in ρ_1, ρ_2, h_1 and h_2 which result from the impression of the stationary, cyclonic storm on the system. The vertically-averaged equations of motion and continuity for the upper and lower layers are:

Upper layer

$$\frac{\partial u_1}{\partial t}+u_1\frac{\partial u_1}{\partial r}-\left(\frac{v_1}{r}+f\right)v_1 = \frac{-1}{\rho_1 h_1}\int_{h_2}^{h_1+h_2}\frac{\partial P_1}{\partial r}dz+\frac{(\tau_r{}^S-\tau_r{}^I)}{\rho_1 h_1}, \quad (1)$$

$$\frac{\partial v_1}{\partial t}+u_1\frac{\partial v_1}{\partial r}+\left(\frac{v_1}{r}+f\right)u_1=\frac{(\tau_\theta{}^S-\tau_\theta{}^I)}{\rho_1 h_1}, \quad (2)$$

$$\frac{\partial \rho_1 h_1}{\partial t}+\frac{1}{r}\frac{\partial}{\partial r}(\rho_1 h_1 u_1 r)=0. \quad (3)$$

Lower layer

$$\frac{\partial u_2}{\partial t}+u_2\frac{\partial u_2}{\partial r}-\left(\frac{v_2}{r}+f\right)v_2 = \frac{-1}{\rho_2 h_2}\int_{0}^{h_2}\frac{\partial P_2}{\partial r}dz+\frac{(\tau_r{}^I-\tau_r{}^B)}{\rho_2 h_2}, \quad (4)$$

$$\frac{\partial v_2}{\partial t}+u_2\frac{\partial v_2}{\partial r}+\left(\frac{v_2}{r}+f\right)u_2=\frac{(\tau_\theta{}^I-\tau_\theta{}^B)}{\rho_2 h_2}, \quad (5)$$

$$\frac{\partial \rho_2 h_2}{\partial t}+\frac{1}{r}\frac{\partial}{\partial r}(\rho_2 h_2 u_2 r)=0. \quad (6)$$

In the above, u and v are the radial and tangential components of velocity for the layer; P, the fluid pressure; and τ^S, τ^I and τ^B, the turbulent shear stresses at the sea surface, ocean interface, and bottom, respectively. The Coriolis parameter f equals $2\Omega\sin\varphi$, where Ω is the angular speed of the Earth and φ is latitude (taken as the latitude at the center of the system).

If the pressure is taken to be hydrostatic in the vertical, the pressure distributions are given by

$$\left.\begin{aligned} P_1&=P_A+\rho_1 g(h_1+h_2-z), && h_2\le z\le h_1+h_2\\ P_2&=P_A+\rho_1 g h_1+\rho_2 g(h_2-z), && 0\le z\le h_2\end{aligned}\right\}, \quad (7)$$

where P_A is the atmospheric pressure at the sea surface and g is the acceleration of gravity. The integrals in (1) and (4) become

$$\frac{1}{\rho_1 h_1}\int_{h_2}^{h_1+h_2}\frac{\partial P_1}{\partial r}dz=\frac{1}{\rho_1}\frac{\partial P_A}{\partial r}+g\frac{\partial(h_1+h_2)}{\partial r}+\frac{g h_1}{2\rho_1}\frac{\partial \rho_1}{\partial r}, \quad (8a)$$

$$\frac{1}{\rho_2 h_2}\int_{0}^{h_2}\frac{\partial P_2}{\partial r}dz=\frac{1}{\rho_2}\frac{\partial P_A}{\partial r}+g\frac{\rho_1}{\rho_2}\frac{\partial h_1}{\partial r}+\frac{g h_1}{\rho_2}\frac{\partial \rho_1}{\partial r}+\frac{g h_2}{2\rho_2}\frac{\partial \rho_2}{\partial r}+g\frac{\partial h_2}{\partial r}. \quad (8b)$$

In the general model, allowance is made for density changes due to turbulent transfer of heat and/or salt between the two ocean layers. As an approximation, the density will be considered to be a linear function of temperature and salinity, i.e.,

$$\rho=\rho_0-aT+bs, \quad (9)$$

where T is temperature, s salinity and ρ_0, a, b are positive constants. Here we neglect variations of ρ_0 with pressure. If we let C represent either s or the specific enthalpy, $c_p T$, then C should satisfy conservation relations of the form

$$\left.\begin{aligned}\frac{\partial(\rho_1 C_1 h_1)}{\partial t}+\frac{1}{r}\frac{\partial}{\partial r}(\rho_1 C_1 h_1 u_1 r)&=-Q_c{}^I\\ \frac{\partial(\rho_2 C_2 h_2)}{\partial t}+\frac{1}{r}\frac{\partial}{\partial r}(\rho_2 C_2 h_2 u_2 r)&=Q_c{}^I\end{aligned}\right\}, \quad (10)$$

where $Q_c{}^I$ is the downward flux density of C at the interface, i.e., the transfer of salt or heat per unit time from the upper to the lower layer.

We assume that the turbulent exchange processes for heat and salt are identical and that

$$Q_c{}^I=B(C_1-C_2), \quad (11)$$

where B is independent of C_1 or C_2. Then if we take an appropriate linear combination of (10), it can be shown that

$$\frac{\partial}{\partial t}[\rho_1(\rho_1-\rho_0)h_1]+\frac{1}{r}\frac{\partial}{\partial r}[\rho_1(\rho_1-\rho_0)h_1 u_1 r] = -B(\rho_1-\rho_2), \quad (12)$$

$$\frac{\partial}{\partial t}[\rho_2(\rho_2-\rho_0)h_2]+\frac{1}{r}\frac{\partial}{\partial r}[\rho_2(\rho_2-\rho_0)h_2 u_2 r] = B(\rho_1-\rho_2). \quad (13)$$

Note that these relations are obtained from principles of conservation of heat and salt; therefore, they are independent of (3) and (6). The variable, $\rho-\rho_0$, essentially corresponds to the quantity σ_t commonly employed in oceanographic analysis.

In summary, Eqs. (1)–(6), (12), (13) represent the general model with the pressure integrals in (1) and (4) determined by (8). The dependent variables, u_1, v_1, h_1, ρ_1; u_2, v_2, h_2, ρ_2, are functions of the independent variables r and t. The quantities, P_A, $\tau_r{}^S$, $\tau_\theta{}^S$, B, are to be prescribed. The functional form of the quantities, $\tau_r{}^I$, $\tau_\theta{}^I$, $\tau_r{}^B$, $\tau_\theta{}^B$, must be chosen.

A simple set of initial conditions is selected. We assume a state of rest and, in addition, each layer is initially of uniform depth and uniform density. Also, we stipulate that u, v, h and ρ have their initial values at $r=\infty$ for each layer and $u=v=0$ at $r=0$.

This is a closed set of non-linear partial differential equations for which there are two possible methods of

solution: 1) linearized perturbation technique and 2) the method of characteristics (Freeman, 1951). Actually, the entire set of equations is quasi-linear, i.e., it involves only first powers of the derivatives of the dependent variables. Since the method of characteristics is best suited for quasi-linear systems with two independent variables, it will be used in determining the solution.

For the general problem involving eight dependent variables there will exist eight characteristic paths of integration in the r,t-plane. Since the system of equations is of hyperbolic character, the characteristic paths are all real.

One can distinguish four different classes of behavior of the general system: a) baroclinic wave modes, b) barotropic wave modes, c) vortex modes, d) mixing modes. In general, all of these modes can co-exist and they are coupled due to the non-linearity of the system and through the influence of rotation of the earth. The barotropic wave modes are characterized by a very large propagational speed compared with that of the baroclinic waves. In the presence of barotropic modes the numerical problem involves at least an order of magnitude greater machine time as compared with certain special cases in which the barotropic mode is filtered from the system at the outset.

3. The specific ocean model

The general set of equations represents a formidable problem. Hence, a series of special problems with increasing complexity was defined. The present work deals with the first of these. In this simple model the lower layer is considered to be infinitely deep which permits it to be considered of constant density and at rest for all r and t. This constraint automatically filters out the barotropic (external) modes of motion and confines attention to the baroclinic (internal) mode of response. We will not consider turbulent mixing between the ocean layers, i.e., ρ_1 is also constant. (The second paper will consider this additional feature.)

Numerical solutions were obtained for $r\geq 0$, $0\leq t<48$ hr. The vertical velocity at the interface w was determined posteriorly using the integrated continuity equation

$$w=-\left[\frac{\partial h}{\partial t}+u\frac{\partial h}{\partial r}\right]. \tag{14}$$

This also follows as a kinematic condition at the interface.

For convenience a density contrast variable ϵ is defined

$$\epsilon\equiv\frac{\rho_2-\rho_1}{\rho_2}. \tag{15}$$

For normal oceanic situations at mid-latitudes, ϵ is of the order of magnitude of 2×10^{-3}.

Consider the general set with $u_2=v_2=0$ and $\epsilon=$ constant and suppress the subscript 1. Since turbulent shear stresses in fluids are found to depend quadratically on velocity, the interior stress τ^I is defined as

$$\left.\begin{aligned}\tau_r{}^I&\equiv\rho Kqu\\ \tau_\theta{}^I&\equiv\rho Kqv\end{aligned}\right\}, \tag{16}$$

where K is a dimensionless and constant coefficient and

$$q\equiv\sqrt{u^2+v^2}. \tag{17}$$

We choose $K=C_D$, the atmospheric drag coefficient; O'Brien (1965) presents a physical argument supporting this choice.

Therefore, the equations of the specific model are:

$$\frac{\partial u}{\partial t}+u\frac{\partial u}{\partial r}-\left(f+\frac{v}{r}\right)v+g\epsilon\frac{\partial h}{\partial r}=(\tau_r{}^S-\rho Kqu)/\rho h, \tag{18}$$

$$\frac{\partial v}{\partial t}+u\frac{\partial v}{\partial r}+\left(f+\frac{v}{r}\right)u=(\tau_\theta{}^S-\rho Kqv)/\rho h, \tag{19}$$

$$\frac{\partial h}{\partial t}+\frac{1}{r}\frac{\partial uhr}{\partial r}=0. \tag{20}$$

The characteristic forms (O'Brien, 1965) of the above are:

$$\frac{d}{dt}(u\pm 2c)=(f+v/r)v+\tau_r{}^S/h-Kqu/h\mp cu/r, \tag{21}$$

along

$$dr/dt=u\pm c, \tag{22}$$

and

$$\frac{d}{dt}(vr+\tfrac{1}{2}fr^2)=r\tau_\theta{}^S/h-rKqv/h, \tag{23}$$

along

$$dr/dt=u, \tag{24}$$

where the baroclinic wave speed c is defined as

$$c\equiv\sqrt{\epsilon gh}. \tag{25}$$

Eqs. (22) and (24) define a family of characteristic curves in the r,t-plane along which the integration of (21) and (23) can be carried out using simple quadrature techniques, thereby avoiding many of the unpredictable errors usually associated with finite difference methods of solving non-linear partial differential equations in their original form.

4. Energy conservation

It is absolutely essential that any numerical technique used to solve the above special model conserve the sum of the kinetic and potential energies. Conservation is used here in the sense that the total energy present in the system must equal the initial energy plus the net gain (or loss) of energy to (or from) the

system. Since it seems impractical to define a linearized model to test the stability of the numerical procedure for this highly non-linear problem, various energy conservation relationships were derived and used to ensure energy balance in the solutions. (The authors found these energy conservation tests to be indispensable for revealing programming errors.)

We will define the total energy E in a unit column by

$$E\equiv\tfrac{1}{2}q^2h+\tfrac{1}{2}g\epsilon h^2, \tag{26}$$

which has the cgs dimensions of ergs $\mathrm{cm}^{-2}\rho^{-1}$. The total energy consists of two parts: 1) the kinetic energy $\frac{1}{2}q^2h$, and 2) the potential energy due to stratification $\frac{1}{2}g\epsilon h^2$. The latter (except for the factor ρ) represents specifically the potential energy in excess of that for a homogeneous column of density ρ_2 which has the same total mass as the stratified column (per unit area). In the usual way, we can combine Eqs. (18)–(20) and obtain

$$\frac{\partial E}{\partial t}+\frac{1}{r}\frac{\partial}{\partial r}[hur(g\epsilon h+\tfrac{1}{2}q^2)]=u\tau_r{}^S+v\tau_\theta{}^S-Kq^3. \tag{27}$$

An energy flux J and an energy supply S are defined by

$$\left.\begin{aligned} J&\equiv hur(g\epsilon h+\tfrac{1}{2}q^2)\\ S&\equiv u\tau_r{}^S+v\tau_\theta{}^S\end{aligned}\right\}. \tag{28}$$

The term $-Kq^3$ is negative definite and represents the dissipation of kinetic energy due to transfer of momentum to the lower layer. Since S may be positive or negative, energy exchange with the atmosphere may be in either direction depending on the sign and relative magnitude of the products $u\tau_r{}^S$ and $v\tau_\theta{}^S$.

We recognize that there are two distinct baroclinic modes inherent in the models and that it is possible to write a separate energy equation for each mode. Let us define a vortex mode with associated energy $\frac{1}{2}v^2h$ and a radially-polarized wave mode with associated energy $(\frac{1}{2}u^2h+\frac{1}{2}\epsilon gh^2)$. The partial energy equations for each mode are

$$\frac{\partial(\frac{1}{2}v^2h)}{\partial t}+\frac{1}{r}\frac{\partial}{\partial r}(\tfrac{1}{2}ruhv^2)=-uvh(f+v/r)+v\tau_\theta{}^S-Kqv^2, \tag{29}$$

$$\frac{\partial(\frac{1}{2}u^2h+\frac{1}{2}\epsilon gh)}{\partial t}+\frac{1}{r}\frac{\partial}{\partial r}[ruh(\epsilon gh+\tfrac{1}{2}u^2)]=uvh(f+v/r)+u\tau_r{}^S-Kqu^2. \tag{30}$$

Clearly the, sum of (29) and (30) yields the total energy equation (27). The term, $uvh(f+v/r)$, represents the coupling mechanism between the two modes. This coupling deserves special comment. We recognize that, in an atmospheric cyclone, $\tau_\theta{}^S>\tau_r{}^S$ in magnitude. Thus, a large portion of the energy supply from the atmosphere will initially dominate the vortex mode. However, the energy of the vortex mode can be transferred to the energy of the wave mode through the coupling term, i.e., through the action of the Coriolis acceleration fv and the centripetal acceleration v^2/r. The latter must be negligible for large r. Thus, near the center of the storm both accelerations may transfer vortex energy to wave energy and vice versa. But, at large radii, only the Coriolis acceleration is effective in the transfer of excess energy from one mode to another. This coupling between the two modes effectively prevents the formation of a bore in the solution (O'Brien, 1965).

5. Hurricane structure

Let us consider a stationary, axially-symmetric hurricane modeled after Hilda, 1964. We need to prescribe a consistent air pressure distribution and wind stress distribution. Following Kajiura (1956), we select the pressure distribution developed by Schloemer (1954). From a sample of nine hurricanes, Schloemer found that a pressure distribution,

$$\frac{P(r)-P_0}{P_n-P_0}=e^{-R/r}, \tag{31}$$

gave an excellent fit to actual data. Here, $P(r)$ is the pressure at radius r, R is the radius of maximum winds, P_0 is the central pressure, and P_n is pressure at the outer periphery of the hurricane. Eq. (31), when differentiated, yields a radial pressure gradient which, in turn, defines a gradient wind speed given f. Since the surface wind is usually found to be 30–40 per cent lower than the gradient wind V_g, the hurricane wind speed V is taken to be 0.7 V_g. In most mature hurricanes, the inflow angle α (the angle between the wind vector and the tangent to the local isobar) tends to be constant in the outer portion of the storm. Near R, α tends to decrease rapidly to zero in the eye. Therefore, we assume that the components of the hurricane wind field are given by

$$\left.\begin{aligned} V_r&=V\beta\sin\alpha_m\\ V_\theta&=V\beta\cos\alpha_m\end{aligned}\right\}, \tag{32}$$

where V_r is the radial component, V_θ the tangential component and α_m the maximum inflow angle at the exterior of the storm. The empirical function β is defined as

$$\beta=\frac{1}{1+10/r^2}, \tag{33}$$

where in (33) only r has the dimension miles.

The components of the turbulent shear stress, $\tau_r{}^S$ and $\tau_\theta{}^S$, are calculated by the relations

$$\left.\begin{aligned} \tau_r{}^S&=\rho_AC_DVV_r\\ \tau_\theta{}^S&=\rho_AC_DVV_\theta\end{aligned}\right\}, \tag{34}$$

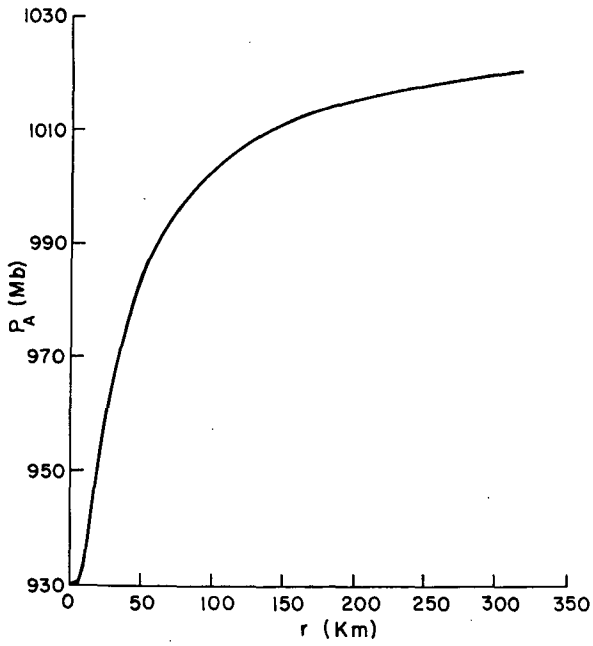

FIG. 2. Hurricane pressure profile along any radial coordinate line.

where C_D is the drag coefficient and ρ_A is air density. The choice of C_D for intense winds is controversial [e.g., Roll (1965)]. Here, the classical value, $C_D = 2.5\times10^{-3}$, is used.

The values of all the physical constants used to characterize the hurricane and ocean model are given in Table 1. The pressure distribution is shown in Fig. 2. The hurricane wind and stress distributions are shown in Fig. 3. A comparison with the actual wind field of Hilda is given by O'Brien (1965). For convenience, the value of τ_r^S and τ_θ^S follow (34) up to 100 mi and then they are decreased linearly to zero at 200 mi. This permits us to designate the forced region, $0<r<200$ mi, as the Storm Region and the region, $r>200$, the Free Region (see Fig. 4). This simplifies the numerical calculations at the outer boundary of the Free Region.

TABLE 1. Values of physical constants and parameters.

Symbol	Value	Description
C_D	2.5×10^{-3}	atmospheric drag coefficient
g	980 cm sec^{-2}	acceleration of gravity
h_0	100 m	initial depth of upper layer
K	2.5×10^{-3}	eddy diffusivity
P_n	1030 mb	air pressure outside the hurricane
P_0	930 mb	central air pressure of the hurricane
R	20 mi	radius of maximum wind
α_m	35 deg	maximum inflow angle
ϵ_0	2.0×10^{-3}	initial density contrast
ρ_A	1.28×10^{-3} gm cm^{-3}	air density
ρ_1	1.0 gm cm^{-3}	water density of upper layer
φ	25N	latitude of storm center
Ω	7.292×10^{-5} sec^{-1}	angular speed of the Earth
Δr	1 mi	radial grid spacing
Δt	18 min	temporal grid spacing

Only the atmospheric distributions of τ_r^S and τ_θ^S, as seen in Fig. 3, are needed for the ocean model.

6. Numerical techniques

The equations for the model, with the boundary conditions shown in Fig. 4, were solved on an IBM 7094 using a numerical form of the method of characteristics. Ordinarily, when this method is used to solve a system of non-linear differential equations, the characteristics for the equations are constructed over the region of known initial data. By proceeding along these lines which lie in the coordinate space, the solutions are determined for later times and new regions of space. However, in this study a modification of the classical method which employs evenly spaced incre-

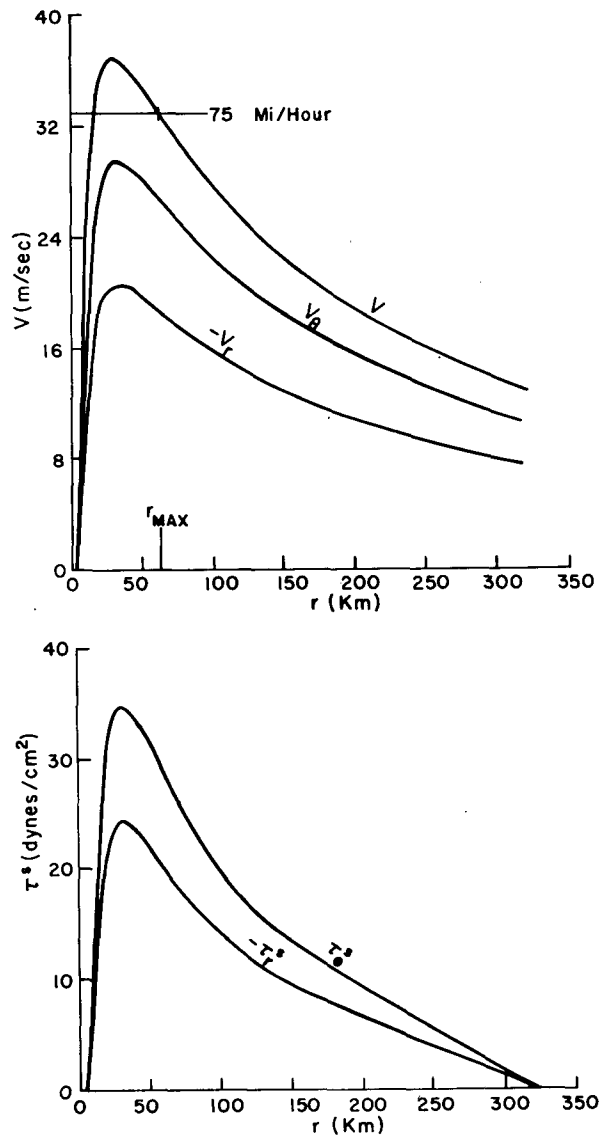

FIG. 3. Hurricane wind and stress distributions along any radius; r_{max} is the maximum radius of hurricane force winds.

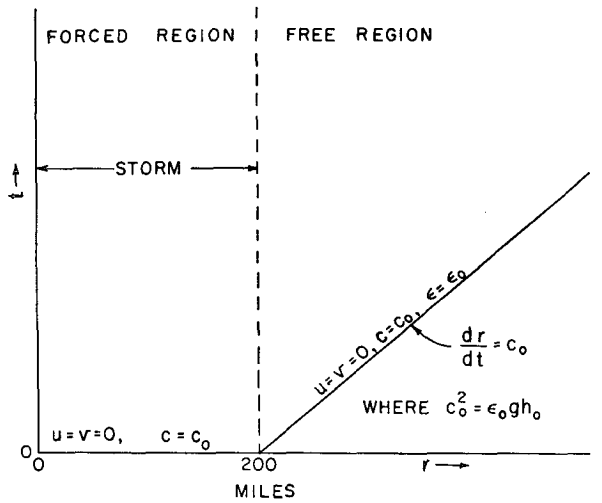

FIG. 4. Schematic drawing of the coordinate space showing the boundary conditions and defining the Forced Region and Free Region.

ments for the independent variables was used. The technique is attributed to Hartree (Fox, 1962).

Consider the grid stencil shown in Fig. 5 which illustrates the point pattern and characteristics used to determine the values of the dependent variables, u, v, h, at an arbitrary grid point $[r_m, t_{k+1}]$. Note that the characteristic lines may be curved and need not intersect the grid points since this is a non-linear problem.

As shown in Fig. 5, the intersection of the positive characteristic, $u+c$, with the previous time level t_k is designated r_A; the intersection of the negative characteristic, $u-c$, r_B; and the intersection of the third characteristic, u, r_C. Hence, using the Trapezoidal Rule for the right-hand sides of (21) through (24), we may write the integrated forms (shown for the positive characteristic) as

$$u_{m,k+1}+2c_{m,k+1}=u_A+2c_A+\frac{\Delta t}{2}[F_{m,k+1}+F_A], \quad (35)$$

$$r_m-r_A=\frac{\Delta t}{2}[u_{m,k+1}+c_{m,k+1}+u_A+c_A], \quad (36)$$

where $\Delta t=t_{k+1}-t_k$ and F is the right-hand side of (21) evaulated at the points $[r_m, t_{k+1}]$ and $[r_A, t_k]$. The integrated equations form a set of six non-linear algebraic equations in the six unknowns, $u_{m,k+1}$, $v_{m,k+1}$, $c_{m,k+1}$, r_A, r_B, r_C. Now, from previous integrations or the initial conditions, we know the values of u, v, h at all the grid points $[r>0, t=t_k]$. Therefore, given an approximation of r_A, r_B and r_C, we can determine estimates of u_A, v_A, etc., using interpolation.

Although linear interpolation would probably suffice, a special technique called "double quadratic interpolation" was used. This method consists simply of using the average result of two quadratic interpolations. For example, in Fig. 5, the value of u_A, given r_A, is found by fitting one parabola to the known values of u at r_{m-2}, r_{m-1}, r_m and a second parabola to the known values of u at r_{m-1}, r_m, r_{m+1}. Each quadratic is then evaluated at r_A and the average result is used as u_A.

Now, given approximations of u, v, h at r_A, r_B, r_C, the integrated equations are solved using the Gauss-Seidel iteration method in which the initial guesses for the unknowns are their values found at the previous time step. The criterion of convergence was that the residual in (35) and its counterpart for the negative characteristic were less than 10^{-5} cm sec^{-1}. Using this criterion, the solutions at each grid point were found in 3-8 cycles. Of course, after each cycle, new estimates of u_A, v_A, etc., were determined at r_A, r_B and r_C.

Special techniques are required at $r=0$ and along the positive characteristic c_0 (see Fig. 4) at the exterior of the storm. Along $r=0$, $u=v=0$ and $\epsilon=\epsilon_0$, but h varies. The new value of $c_{0,k+1}$ was found by solving the counterpart of (35) for the negative characteristic and the integrated form of $dr/dt=u-c$ for the two unknowns, r_B and $c_{0,k+1}$. The values of u, v, etc., needed at "negative" r for the double interpolation scheme were found using the principle of reflection on the velocities at the positive grid points.

At the exterior of the storm, we used an expanding grid and integrated to the new value of c_0. Actually, it was not necessary to calculate where c_0 existed for a particular time step, but just integrate until both velocity components were zero.

7. Results

The characteristic equations (21) through (24) were integrated numerically using the techniques just outlined. These computations yielded values of u, v and h at evenly spaced grid points in the Forced and Free Regions (Fig. 4) for $0<t<48$ hr. These data are shown for 90-min intervals in Figs. 6, 7 and 8. Smooth curves were drawn through the data points. Each curve is based on 300 computed values.

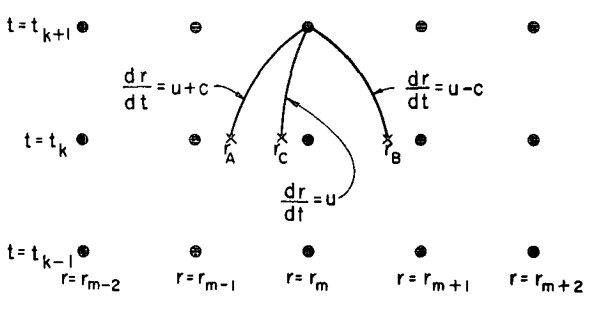

GRID STENCIL AND CHARACTERISTICS

FIG. 5. Point pattern in the coordinate space showing a possible configuration of the three characteristic lines through an arbitrary grid point $[r_m, t_{k+1}]$.

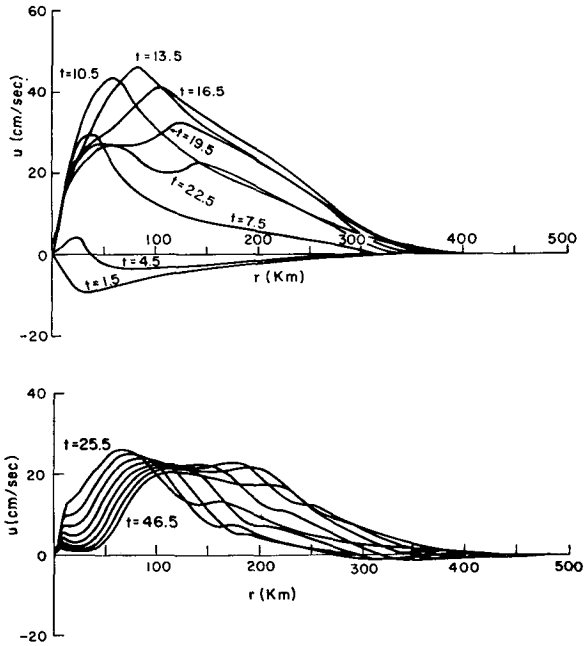

FIG. 6. Radial velocity u as a function of r and t; top diagram, 0–24 hr; bottom diagram, 24–48 hr. Each curve is labeled t(hr) from $t=0$.

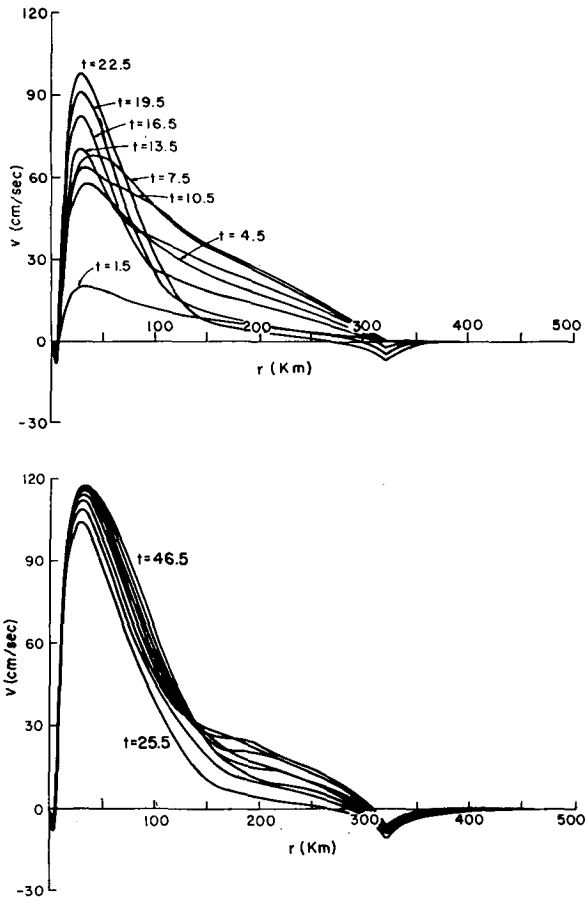

FIG. 7. Tangential velocity v as a function of r and t; top diagram, 0–24 hr; bottom diagram, 24–48 hr.

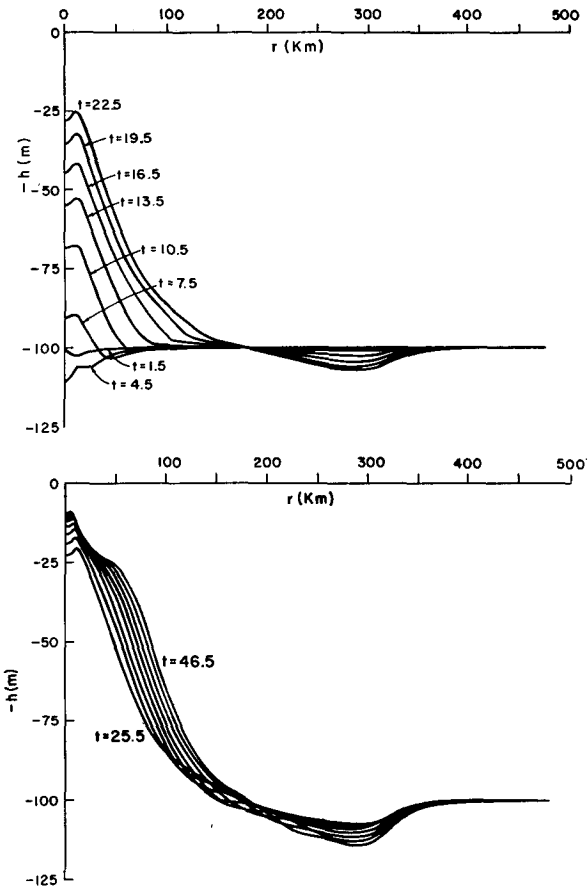

FIG. 8. Depth of upper layer h as a function of r and t; top diagram, 0–24 hr; bottom diagram, 24–48 hr. Note that $h>0$, but is shown as $-h$ for illustrative purposes.

There is a surprising amount of fine structure in the velocities which would require lengthy description. However, there are a few noteworthy features:

a) The initial radial velocity u is negative since $\tau_r{}^S<0$ for all r.

b) The initial tangential velocity v is positive since $\tau_\theta{}^S>0$ for all r.

c) After approximately 3 hr, the radial velocity changes sign near the center due to the action of the terms, v^2/r and fv.

d) A series of radial dispersive waves forms near 30 km and propagates outward. (Two are easily distinguishable.)

e) The tangential velocity becomes approximately stationary after 24 hr inside 20 km.

f) A narrow, stationary anticyclonic vortex forms beneath the eye of the storm.

g) After 12 hr, the profiles of v mirror the profile of $\tau_\theta{}^S$.

h) A permanent anticyclonic vortex forms at 320 km (the border between the Forced and Free Regions.) This is an artificial feature introduced by the distribution of τ^S (i.e., the rather sudden cutoff at 200

mi) and the monotonic decreasing nature of u along the majority of the later profiles.

The strong upwelling created by the velocity divergence is shown in Fig. 8. Here, for illustrative purposes, the profiles of h are shown as if each profile represented the configuration of the bottom of the layer which was initially at 100 m everywhere. The noteworthy features are:

a) The initial response ($u<0$) of the system causes a thickening (downwelling) in the center of the system.

b) When u becomes positive near the center, the water is swept from the center and h decreases rapidly within $r<80$ km.

c) The maximum upwelling occurs at approximately 30 km, which is an expected response to the maximum value of τ^S.

d) During the second 24 hr, the rate of upwelling diminishes. This evidence of numerical stability is an indication of a degree of physical reality in the model. We may imagine that the cold dense sea water of the lower layer rose in the area of upwelling to replace the lighter surface water which was removed from the central region. The displaced warmer waters accounted for the thickening of the upper layer between 80 and 300 km.

The vertical velocity w was determined from the values of u and h using a finite difference form of Eq. (14). The profiles of w (Fig. 9) show that:

a) Initially, w is negative near the center.

b) After 4 hr, w becomes positive near the center and reaches a maximum of 0.25 cm sec^{-1} after 7 hr.

c) As h approaches zero near the center, w diminishes rapidly.

8. Comparison with observations

The only observations with which we can compare the present work are those of Leipper (1967). However, first it is necessary to understand to what degree the model ocean approximates the real ocean. It is recognized that the density and the velocity of the real ocean vary continuously with depth. In the present model, we have approximated the density structure before the hurricane with two uniform layers. The equations of motion have been integrated with respect to depth. Hence, the velocity components are considered as the depth-averaged velocity components for the layer. *A priori*, we have assumed that the initial dynamic response of the real ocean would be to stir the upper portion of the ocean. This stirring will produce a well-mixed layer and will usually lead to a temperature drop at the surface. In the simple model described here, it is assumed, as a first approximation, that only the upper 100 m of the ocean will then respond to the hurricane's wind field.

It is our intent to compare the results of the theoretical model with the actual observations in order to lend some confidence to the results.

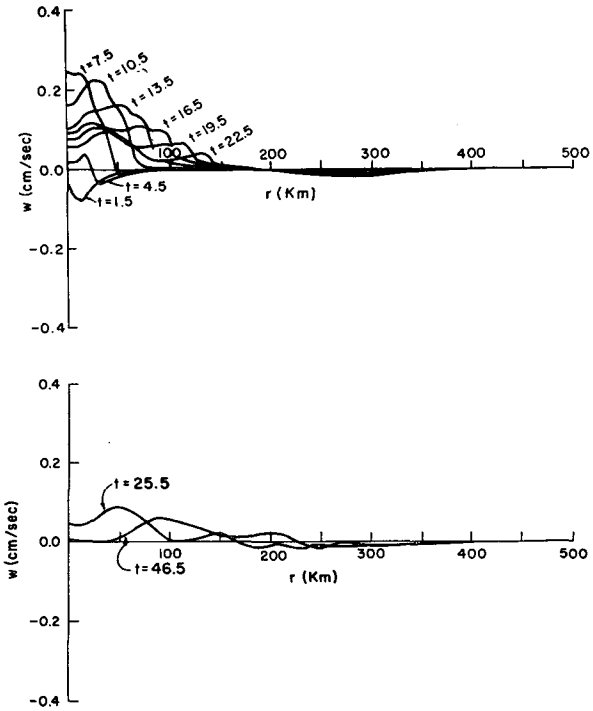

FIG. 9. Vertical velocity w as a function of r and t; top diagram, 0–24 hr; bottom diagram, 24–48 hr. Each curve is labeled t(hr) from $t=0$.

When we compare Leipper's Figs. 12b and 12e we find that considerable upwelling is evident. There is a shallow mixed layer less than 25 m deep along the hurricane path and a deeper mixed layer (60–80 m) at the edges of the section. The upwelled area extends 100–150 km on each side of the hurricane path. In his Fig. 14b the Sigma-t surfaces show a similar structure, i.e., strong evidence of upwelling along the hurricane track, a shallow mixed layer in the center, and a deeper mixed layer at the edges of the section. In this figure there is evidence that the strongest upwelling is not exactly in the center but slightly displaced, e.g., consider the lines $\sigma_t=26$.

Let us recall some of the results (say Fig. 8) of the present work which are similar to the structure along section CC′:

a) On the first day, the upwelling is confined to the region of hurricane force winds.

b) Upwelling produces a shallow mixed layer in the center and a deeper mixed layer outside the center.

c) The maximum upwelling is slightly off center.

Although section CC′ does not conclusively show an area of downwelling between 80–300 km of the center, as found in the present results, there is some evidence that the downwelling does occur. By comparing the ocean configuration in the eastern Gulf of Mexico prior to and following Betsy, 1965, Leipper[2] finds that

[2] To be published.

the distribution of oxygen indicates an area of downwelling adjacent to the central upwelling region. The upwelling found after Betsy was not as marked as that after Hilda. This is attributed to the fact that Betsy moved rapidly through the eastern Gulf of Mexico and passed over a large ocean eddy current in the region of observations.

9. Comments on previous theoretical work

Hidaka and Akiba (1955) studied the steady-state upwelling due to a stationary cyclone with a maximum wind stress of 1 dyne cm^{-2}. Clearly, it is not entirely permissible to compare the present transient models with a steady-state model. However, we can make a few comparisons. First, in the present problem, we find approximate steady-state velocities only after one day and within the radius of maximum wind stress. Second, Hidaka and Akiba find a maximum vertical velocity of 2.4×10^{-3} cm sec^{-1}. If we increase their maximum vertical velocity (or wind stress) 50-fold, we obtain a value of w comparable to that observed in the present work. Third, they find that the upwelling is confined to within twice the radius of maximum wind stress, a result similar to both the present work and Leipper's observations.

Ichiye (1955) solves a transient problem similar to the present work. However, for the purpose of evaluating the vertical velocity via the vorticity equation, he assumes that the current fluxes are given by the Ekman relations,

$$uh=\tau_\theta{}^S/f\rho, \quad vh=-\tau_r{}^S/f\rho. \tag{37}$$

This approximation is not supported by the present work. The right-hand side is constant in both problems, but in the present problem the left-hand side is definitely not constant (not illustrated). In fact, the radial current flux even differs in sign at those places where u is negative, e.g., during the first few hours in each of the present models.

On the positive side, Ichiye finds that the maximum w, induced by a stationary cyclone with maximum wind speed of 29.7 m sec^{-1}, is 0.5 cm sec^{-1}. In addition, the upwelling is confined to within twice the radius of maximum wind stress. Both of these results agree with the present research.

An obvious extension of the present work is the investigation of an axially-symmetric cyclone moving at a constant velocity U. Following Kajiura (1956), a choice of independent variables would be $x-Ut$ and y, where x and y are Cartesian coordinates. The moving hurricane problem is fundamentally distinct from the stationary model and the method of analysis by characteristics may be of limited value.

There are other immediately feasible extensions of the present study. Future work might include consideration of a finite lower layer, multiple layers, bottom topography, etc. Also, the physical exchange of heat and moisture with the atmosphere could be studied. There appears to be ample extensions for future work, however, the pertinent and detailed observations needed to confirm the theoretical work will be difficult to obtain.

10. Summary

It has been demonstrated that the simple model approximates the structure of the intense upwelling found after hurricane Hilda to a reasonable degree. The active upwelling is confined to the central portion of the Forced Region. The initial response of the ocean results in a thickening of the upper layer at the center. However, after several hours significant velocity divergence develops and the warm central waters are displaced, which permits strong upwelling in the center of the system.

One may logically inquire into how permanent will be the observed density configuration created by the intense upwelling. In nature, we can assume that, in the absence of a moderately-strong, externally-driven ocean circulation, the kinetic energy remaining in the upper layer of the real ocean will be quickly dissipated. This will leave a quasi-permanent upwelled region which may be identifiable for several weeks after the hurricane's passage.

Acknowledgments. We wish to thank Prof. Dale F. Leipper for his continuous encouragement and advice. The Texas A&M University Data Processing Center provided the extensive computer time required for this research. The Office of Naval Research, Contract Nonr-2119(04), provided data, staff and clerical assistance. One of us (J. O'B.) was supported by National Aeronautics and Space Adminstration and Graduate College Fellowships during the completion of this work which is contained in part in his Ph.D. dissertation. The National Center for Atmospheric Research provided the support for preparing the final publication copy of this paper.

List of Symbols

a, b	positive constants defined by Eq. (9)
B	mixing coefficient defined by Eq. (11)
c	wave speed, defined by Eq. (25)
c_0	initial wave speed
C_D	atmospheric drag coefficient
C, C_1, C_2	salinity or specific enthalpy defined by Eq. (10)
c_P	specific heat of sea water at constant pressure
E	total energy in a unit column, Eq. (26)
f	Coriolis parameter
F	right-hand side of (21), see (35)
g	acceleration of gravity
h, h_1, h_2	thickness of an ocean layer
h_0	initial thickness of upper layer

J	energy flux density defined by Eq. (28)
K	internal momentum exchange coefficient, Eq. (16)
P, P_A	pressure at radius r in hurricane
P_0	central pressure of hurricane
P_n	pressure outside of hurricane
P_1, P_2	ocean pressure
q	magnitude of velocity, Eq. (17)
$Q_C{}^I$	flux density of C between ocean layers, Eq. (11)
r	independent radial coordinate, increasing outward
r_A, r_B, r_C	intersections at t_k in Fig. 5
$r_{\max}$	maximum radius of hurricane force winds
R	radius of maximum wind
s	salinity
S	energy supply from atmosphere defined by Eq. (28)
t	independent temporal coordinate
t_k, t_{k-1}, t_{k+1}	arbitrary time levels used in Fig. 5
T	temperature
u, u_1, u_2	radial velocity in ocean
U	translational speed of hurricane
v, v_1, v_2	tangential velocity in ocean
V_g	gradient wind in hurricane
V, V_r, V_θ	magnitude and components of surface wind speed at 10 m above ocean
w	vertical velocity in ocean
z	independent vertical coordinate, increasing upward
α	inflow angle in hurricane
α_m	maximum inflow angle
β	empirical function defined by Eq. (32)
Δr, Δt	grid intervals
ϵ	density contrast defined by Eq. (15)
θ	independent azimuth coordinate
ρ_A	air density
ρ, ρ_1, ρ_2, ρ_0	sea densities
σ_t	Sigma-t
τ^S, $\tau_r{}^S$, $\tau_\theta{}^S$	wind stress magnitude and components at sea surface
τ^I, $\tau_r{}^I$, $\tau_\theta{}^I$	magnitude and components of internal shearing stress at the interface
$\tau_r{}^B$, $\tau_\theta{}^B$	shearing stress components at the sea bed
φ	latitude of storm center
Ω	angular speed of the Earth

REFERENCES

Fisher, E. L., 1958: Hurricanes and the sea-surface temperature field. *J. Meteor.*, **15**, 328–333.

Fox, L., 1962: *Numerical Solution of Ordinary and Partial Differential Equations*. London, Addison-Wesley, 339–342.

Freeman, J. C., 1951: The solution of non-linear meteorological problems by the method of characteristics. *Compendium of Meteorology*, Boston, Amer. Meteor. Soc., 421–433.

Hidaka, K., and Y. Akiba, 1955: Upwelling induced by a circular wind system. *Records Oceanog. Works Japan*, **2**, 7–18.

Ichiye, T., 1955: On the variation of oceanic circulation (V). *Geophys. Mag.*, **26**, 283–342.

Jordan, C. L., 1964: On the influence of tropical cyclones on the sea surface temperature field. *Proc. Symp. Trop. Meteor.*, New Zealand Meteor. Service, Wellington, 614–622.

Kajiura, K., 1956: A forced wave caused by atmospheric disturbances in deep water. Tech. Report 133-1, A&M College of Texas, Ref. 56-26T, 32 pp.

Leipper, D. F., 1967: Observed ocean conditions and hurricane Hilda, 1964. *J. Atmos. Sci.*, **24**, 182–196.

O'Brien, J. J., 1965: The non-linear response of a two-layer, baroclinic ocean to a stationary, axially-symmetric hurricane. Tech. Report, Ref. 65-34T, Texas A&M University, 99 pp.

Roll, H. V , 1965: *Physics of the Marine Atmosphere*. New York, Academic Press, 152–160.

Schloemer, R. W., 1954: Analysis and synthesis of hurricane wind patterns over Lake Okeechobee, Florida. Hydrometeorological Rept., No. 31, U. S. Weather Bureau, 49 pp.